resulted in confidently identifying vortices of different types in measurements of the magnetic-field-induced superfluid density anisotropy in ^{3}He-B. A study of the relaxation of HPDs enabled a systematic measurement of magnetic relaxation parameters [30]. With its property of a spatially uniform order parameter distribution (texture), the homogeneously precessing domain can be effective in studying texture-sensitive phenomena. In particular, the use of the HPD has permitted Leggett frequency measurements in the B-like ^{3}He phase in an aerogel, whose effect on the texture makes standard NMR methods difficult to use for this purpose [31].

8. Conclusion

In summary, the studies reviewed prove the existence of spin supercurrents in ^{3}He-B and demonstrate the analogy between spin superfluidity on the one hand and 'usual' mass superfluidity and superconductivity on the other. As a result, many experiments were explained and new research directions identified. For example, the electric field should play the same role for spin supercurrent that the magnetic field vector-potential does for superconducting electrons. Although very small in magnitude, this effect can in principle be measured. Also of interest might be to conduct research at ultralow temperatures of around 100 μK, where, even though spin supercurrents are clearly important, very long (of the order of an hour) induction signals are observed which the HPD formation model fails to describe [32]. The homogeneously precessing domain was observed not only in ^{3}He-B but also in the B-like phase of ^{3}He in an aerogel — which, in particular, supports interpreting this phase as the analog of the B-phase of the 'usual' bulk ^{3}He as well as opens new possibilities for its study [33].

Dissipationless (reactive) spin currents can exist in other magnetic systems. At sufficiently low temperatures and high magnetic fields, the effective spin diffusion coefficient in Fermi liquids becomes complex, allowing for dissipationless spin currents [34] and thereby leading to a number of phenomena, some of which are analogous to those observed in ^{3}He-B [35, 36]. For example, normal liquid ^{3}He and ^{3}He$-^4$He solutions were observed to exhibit a structure of two oppositely magnetized domains with an in-phase precessing domain wall [37, 38]. In principle, similar phenomena can also occur in magnetically ordered solids. This requires, in addition to the small magnetic relaxation, that the order parameter be degenerate with respect to one of its orientation angles and that the corresponding gradient term be present in the Hamiltonian. Magnetically ordered solid ^{3}He [39] and antiferromagnet $CsNiCl_3$ [40] are candidate materials for such studies.

References

1. Vollhardt D, Wölfle P *The Superfluid Phases of* ^{3}He (London: Taylor & Francis, 1990)
2. Mineev V P *Usp. Fiz. Nauk* **139** 303 (1983) [*Sov. Phys. Usp.* **26** 160 (1983)]
3. Abragam A, Goldman M *Nuclear Magnetism: Order and Disorder* (Oxford: Clarendon Press, 1982) [Translated into Russian (Moscow: Mir, 1984)]
4. Osheroff D D et al. *Phys. Rev. Lett.* **29** 920 (1972)
5. Borovik-Romanov A S, Bunkov Yu M *Sov. Sci. Rev. Sec. A Phys.* **15** 1 (1990)
6. Fomin I A, in *Helium Three* (Modern Problems in Condensed Matter Sciences, Vol. 26, Eds W P Halperin, L P Pitaevskii) (Amsterdam: North-Holland, 1990) p. 609
7. Bunkov Yu M, in *Progress in Low Temperature Physics* Vol. 14 (Ed. W P Halperin) (Amsterdam: Elsevier Sci. Publ., 1995) p. 69
8. Dmitriev V V, Fomin I A *J. Low Temp. Phys.* **135** 361 (2004)
9. Leggett A J *Ann. Phys.* (New York) **85** 11 (1974)
10. Leggett A J, Takagi S *Ann. Phys.* (New York) **106** 79 (1977)
11. Brinkman W F, Smith H *Phys. Lett. A* **53** 43 (1975); Osheroff D D, Corruccini L R, in *Proc. of the 14th Intern. Conf. on Low Temperature Physics, LT-14* Vol. 1 (Eds M Krusius, M Vuorio) (Amsterdam: North-Holland, 1975) p. 100
12. Fomin I A *Zh. Eksp. Teor. Fiz.* **93** 2002 (1987) [*Sov. Phys. JETP* **66** 1142 (1987)]
13. Fomin I A *Pis'ma Zh. Eksp. Teor. Fiz.* **40** 260 (1984) [*JETP Lett.* **40** 1037 (1984)]; *Zh. Eksp. Teor. Fiz.* **88** 2039 (1985) [*Sov. Phys. JETP* **61** 1207 (1985)]
14. Corruccini L R, Osheroff D D *Phys. Rev. B* **17** 126 (1978)
15. Giannetta R W, Smith E N, Lee D M *J. Low Temp. Phys.* **45** 295 (1981)
16. Borovik-Romanov A S et al. *Pis'ma Zh. Eksp. Teor. Fiz.* **40** 256 (1984) [*JETP Lett.* **40** 1033 (1984)]
17. Borovik-Romanov A S et al. *Zh. Eksp. Teor. Fiz.* **88** 2025 (1985) [*Sov. Phys. JETP* **61** 1199 (1985)]
18. Borovik-Romanov A S et al. *Zh. Eksp. Teor. Fiz.* **96** 956 (1989) [*Sov. Phys. JETP* **69** 542 (1989)]
19. Borovik-Romanov A S et al. *Pis'ma Zh. Eksp. Teor. Fiz.* **45** 98 (1987) [*JETP Lett.* **45** 124 (1987)]
20. Borovik-Romanov A S et al. *Jpn. J. Appl. Phys.* **26** 175 (1987)
21. Borovik-Romanov A S et al. *Phys. Rev. Lett.* **62** 1631 (1989)
22. Fomin I A *Pis'ma Zh. Eksp. Teor. Fiz.* **45** 106 (1987) [*JETP Lett.* **45** 135 (1987)]
23. Borovik-Romanov A S et al. *Pis'ma Zh. Eksp. Teor. Fiz.* **47** 400 (1988) [*JETP Lett.* **47** 478 (1988)]
24. Fomin I A *Zh. Eksp. Teor. Fiz.* **94** (11) 112 (1988) [*Sov. Phys. JETP* **67** 1148 (1988)]
25. Borovik-Romanov A S et al. *Physica B* **165–166** 649 (1990)
26. Bunkov Yu M, Dmitriev V V, Mukharskii Yu M *Physica B* **178** 196 (1992)
27. Bunkov Yu M, Hakonen P J *J. Low Temp. Phys.* **83** 323 (1991)
28. Kondo Y et al. *Phys. Rev. Lett.* **67** 81 (1991)
29. Korhonen J S et al. *Phys. Rev. B* **46** 13983 (1992)
30. Bunkov Yu M et al. *Phys. Rev. Lett.* **65** 867 (1990)
31. Dmitriev V V et al. *Pis'ma Zh. Eksp. Teor. Fiz.* **79** 612 (2004) [*JETP Lett.* **79** 499 (2004)]
32. Bunkov Yu M et al. *Phys. Rev. Lett.* **69** 3092 (1992)
33. Dmitriev V V et al. *Pis'ma Zh. Eksp. Teor. Fiz.* **76** 371 (2002) [*JETP Lett.* **76** 312 (2002)]
34. Leggett A J, Rice M J *Phys. Rev. Lett.* **20** 586 (1968); Leggett A J *J. Phys. C: Solid State Phys.* **3** 448 (1970)
35. Fomin I A *Physica B* **210** 373 (1995)
36. Dmitriev V V, Fomin I A *Pis'ma Zh. Eksp. Teor. Fiz.* **59** 352 (1994) [*JETP Lett.* **59** 378 (1994)]
37. Dmitriev V V, Zakazov S R, Moroz V V *Pis'ma Zh. Eksp. Teor. Fiz.* **61** 309 (1995) [*JETP Lett.* **61** 324 (1995)]; Dmitriev V V, Moroz V V, Zakazov S R *J. Low Temp. Phys.* **101** 141 (1995)
38. Dmitriev V V et al. *Physica B* **210** 366 (1995)
39. Fomin I A, Shopova D V *Pis'ma Zh. Eksp. Teor. Fiz.* **42** 162 (1985) [*JETP Lett.* **42** 199 (1985)]
40. Mineev V P *Zh. Eksp. Teor. Fiz.* **110** 2211 (1996) [*JETP* **83** 1217 (1996)]

PACS numbers: **75.10.–b**, **75.25.+z**, 75.50.Ee
DOI: 10.1070/PU2005v048n01ABEH002112

New magnetic states in crystals

S S Sosin, L A Prozorova, A I Smirnov

1. Introduction

One of the major types of magnetic interactions in crystals is the exchange interaction, which is usually described by a

Heisenberg Hamiltonian of the form

$$\hat{\mathcal{H}} = J\hat{S}_1\hat{S}_2\,, \tag{1}$$

where the exchange integral J is determined by the electron shell overlap of interacting ions, and $\hat{S}_1$ and $\hat{S}_2$ are spin operators. The Hamiltonian of the system of many magnetic ions is written as the sum of pair interactions. Depending on the sign of J, the total ground-state spin of the system takes either a maximum ($J < 0$) or minimum ($J > 0$) value. In the former case, the ground state is a ferromagnetic state of the type $|\uparrow\uparrow\ldots\rangle$, which can occur in crystal structures of any dimensionality and symmetry. Various and diverse properties of ferromagnets have been studied intensively throughout the past century.

For the positive exchange integral, the situation is less trivial. First, the classical (so-called Néel) minimum-spin state $|\uparrow\downarrow\uparrow\downarrow\ldots\rangle$ turns out to be not an eigenstate and can therefore only be considered as an approximation. However, for three-dimensional antiferromagnets the deviation of the ground state from this state — zero-point oscillations of the order parameter — manifests itself only in spin reduction form, meaning that the ordered spin component becomes smaller than the total spin of the ions, $\langle S\rangle/S < 1$. Reducing the dimensionality of the system increases the role of the zero oscillations, leading in the case of a one-dimensional spin chain to a completely destroyed long-range magnetic order. The ground state of a spin chain is a singlet one, with the average spin projection vanishing at each site, $\langle S_i^z\rangle = 0$. In spin-1/2 chains antiferromagnetic correlations fall off with a power law and the excitation spectrum has no gap and close to $\mathbf{k} = 0$ is similar to the spin wave spectrum in an ordinary antiferromagnet [1]. For spin-1 chains, the excitation spectrum is separated from the ground state by an exchange gap, $\Delta \sim 0.4J$, and the correlations decrease exponentially [2]. Due to the presence of the gap, magnetic excitations freeze out at low temperatures $T \ll \Delta$, bringing the magnetic heat capacity and susceptibility to zero. Section 2 discusses one interesting consequence of such a state in antiferromagnets.

Another important difference between antiferromagnetic systems and ferromagnets is the possibility of a geometric exchange frustration, i.e., the peculiar arrangement of magnetic ions in the crystal, which prevents the interacting spins from simultaneously aligning antiparallel. As a consequence, a non-collinear spin structure whose ground state energy exceeds that of the collinear magnet (weak frustration) may form and in some cases makes long-range order completely unachievable (strong frustration), allowing a fundamentally new strong-correlated state — the so-called collective paramagnet — which remains disordered to temperatures $T \ll JS^2/k_{\mathrm{B}}$ [3]. Sections 3 and 4 examine some unusual properties of noncollinear (triangular) antiferromagnets and discuss the major thermodynamic consequence the strongly frustrated exchange interaction has for the particular case of a pyrochlore lattice magnet.

2. Impurity-induced magnetic order in a spin-gap magnet

There is a number of spin-gap systems other than quasi-one-dimensional integer spin chains, including ladder structures [4], dimer systems [5], and alternating-exchange chains. In the last case, as a result of the translational crystal symmetry breaking (the doubling of the lattice spacing), the exchange integral of neighboring ions in the chain alternately changes between two values, $J \pm \delta$. Alternating spin chains may be due to crystal structure [6], but they may also spontaneously result from the so-called spin-Peierls transition, which occurs as a consequence of an exchange energy gain due to dimerization [7, 8]. As a result, the excitation spectrum of a spin-1/2 chain acquires a gap whose magnitude depends on the alternation parameter $\Delta \simeq \delta$ [9] and whose presence leads, as in the case of spin-1 chains, to a finite correlation length $\xi \simeq v\hbar/\Delta$. Being stable to small perturbations like anisotropy and interchain exchange interaction, such a state can be artificially destroyed by nonmagnetic doping. Substituting a nonmagnetic ion for a magnetic one breaks up the spin chain and destroys the singlet state, with the result that regions of antiferromagnetically correlated nonzero average spin projections — i.e., regions of local antiferromagnetic order — form near the impurity atoms. We will call such antiferromagnetic regions clusters. Note that these clusters are formed by the spins of the main matrix against the background of a singlet (i.e., nonmagnetic) state. The number of magnetic ions in a cluster is on the order of ξ/a (a is the interatomic spacing), and the absolute value of the average spin projection has a maximum close to the ends of the chain and decreases in the middle. The cluster has nonzero spin and magnetic moment. For spin-Peierls magnets, the formation of clusters with local antiferromagnetic ordering is considered theoretically in Ref. [10]. The appearance of clusters leads to an unusual phenomenon — the impurity induced antiferromagnetic ordering.

This effect was predicted in Ref. [11] and later observed in spin-Peierls [12] and Haldane [13] magnets and in a dimer spin system [14]. The reason why introducing nonmagnetic impurities leads to magnetic order is that the ends of clusters overlap and that clusters in neighboring chains are correlated by a weak interchain coupling. The resulting order parameter appears to be strongly non-uniform.

Impurity-stimulated magnetic order is conveniently studied using the non-organic spin-Peierls magnet $CuGeO_3$, with a spin-Peierls transition temperature of $T_{\mathrm{SP}} = 14.5$ K and a low-temperature spin gap of $\Delta(0) \simeq 25$ K [7]. The spin gap opens at the temperature T_{SP} and approaches a maximum value $\Delta(0)$ below 7 K. The magnetic ions Cu^{2+} ($S = 1/2$) can be substituted with, for example, nonmagnetic ions of Zn and Mg. These impurities occupy the sites of the Cu^{2+} ions in the $CuGeO_3$ with a solubility limit of higher than 6%. Thus, one can control the number of breaks introduced to the dimerized spin chain. Contributions from chain breaks to the susceptibility and magnetic resonance signals are clearly visible against the background of the singlet and nonmagnetic matrix.

The magnetic resonance signal at the antiferromagnetic phase transition usually transforms from the paramagnetic resonance signal to an antiferromagnetic resonance (AFMR) signal. While the paramagnetic resonance frequency is determined by the properties of isolated magnetic ions, the AFMR frequency depends on order parameter oscillations. Thus, a phase transition to the ordered state is accompanied by a transformation of the magnetic resonance spectrum. The observation of this transformation allows one to obtain the temperature and other characteristics of the transition. At high enough impurity concentrations (above 3%) impurity ions are a small distance (on the order of the correlation length ξ) apart. For such concentrations, the transition to the antiferromagnetic state in $Cu_{(1-x)}Mg_xGeO_3$ is somewhat analogous to the phase transition in ordinary 3D antiferro-

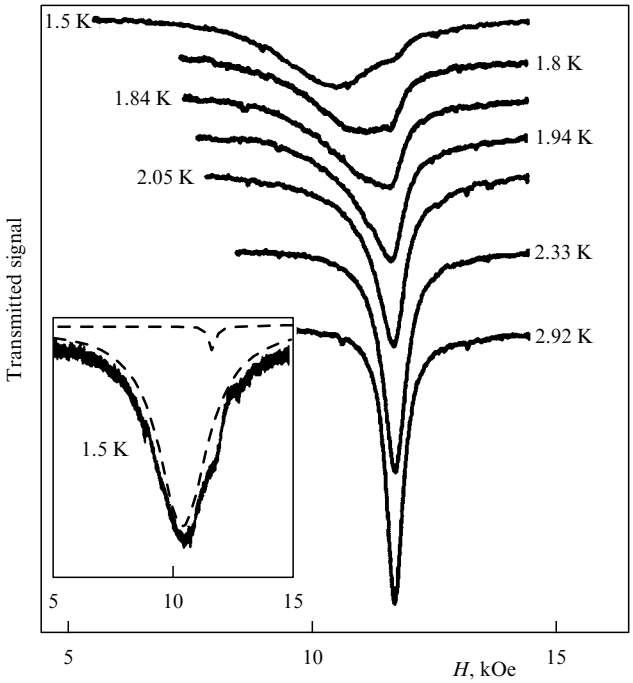

Figure 1. Change in the shape of magnetic resonance line in the vicinity of the Néel temperature in a single crystal of $Cu_{(1-x)}Mg_xGeO_3$: $H \parallel b$, $\nu = 36$ GHz, $T_N = 2.25$ K. Inset shows the expansion of the resonance line at $T = 1.5$ K by two Lorentzian absorptions (dashed lines).

magnets. Of particular interest is the low concentration case, where impurity atoms in a chain are spaced by a distance exceeding the length ξ and spin clusters are separated by remains of the singlet matrix. The process of transition to the antiferromagnetic state as the temperature is decreased was studied in Ref. [15] using the magnetic resonance, a technique which detects both the paramagnetic and antiferromagnetic phases spectroscopically, based on the difference of their resonance frequencies. The experiments were conducted on single crystals of $Cu_{(1-x)}Mg_xGeO_3$ with impurity concentration distributed uniformly to within 10^{-3} over a sample.

Figure 1 follows the evolution of the magnetic resonance spectrum at the transition through the Néel point in doped spin-Peierls magnet $Cu_{(1-x)}Mg_xGeO_3$ with $x = 0.017$. As the temperature decreases, the paramagnetic resonance line splits into two. The first component corresponds to a paramagnetic resonance, the (temperature-independent) resonance field being equal to that of the paramagnetic phase. The resonance field of the second component depends on the temperature, and its frequency-field dependence (see Ref. [15]) corresponds to the spectrum of a biaxial antiferromagnet. There is a wide temperature range where the antiferromagnetic and paramagnetic resonance lines are observed simultaneously. The uniform distribution of impurities over the sample, together with a small transition temperature interval (0.1 K), rule out explaining this coexistence in terms of the macroscopic nonuniformity of the sample. Two simultaneously present resonance modes cannot be explained in the framework of a single-phase examination because order parameter oscillations corresponding to the antiferromagnetic phase rule out the paramagnetic resonance mode and because the paramagnetic phase can even less allow the line to be split. A possible explanation is the macroscopic phase separation of a sample into paramagnetic and antiferromagnetic regions. Let us consider the spin clusters that form around impurity atoms and assume that coherent antiferromagnetic order exists in a region of diameter L^* estimated from the relation

$$k_B T \sim JS^2 \exp\left(-\frac{2L^*}{\xi}\right). \tag{2}$$

At distances larger than L^* antiferromagnetic correlations are destroyed by thermal fluctuations. The antiferromagnetic correlation distances in transverse directions are determined by corresponding exchange integrals. Then we arrive at a simple model of Ref. [15], with an elliptic-shaped antiferromagnetic region around each impurity center. The length of the ellipse along the chain is estimated from Eqn (2), and its transverse dimension is shorter in proportion to the exchange integral ratio. At high temperature the regions of local antiferromagnetic order are small in size and do not touch one another, long-range order is absent, and the cluster contribution to the susceptibility and the magnetic resonance signal is due to each of the clusters having a total magnetic moment — the reason why the susceptibility and the magnetic resonance frequency have a paramagnetic character. As the temperature is lowered, the clusters increase in size and some of them start touching each other, with the result that more extended regions of coherent antiferromagnetic order — ones containing several impurity atoms — appear. Finally, as shown in Fig. 2, an ordered region stretching throughout the entire sample forms, which corresponds to the percolation threshold for a system of interpenetrating spheres [16]. At and around the percolation value L^* (see Fig. 2) the sample still contains single clusters that are isolated from large antiferromagnetic regions by a weakly perturbed singlet matrix. The free spins of these clusters produce paramagnetic resonance signals in the same way they do above the critical point. Thus, there are three types of regions below the Néel temperature: (1) large enough regions of magnetic order which produce AFMR signals, (2) regions of singlet matrix which have no magnetic response, and (3) single clusters, which are separated from the antiferromagnetic regions by the singlet matrix.

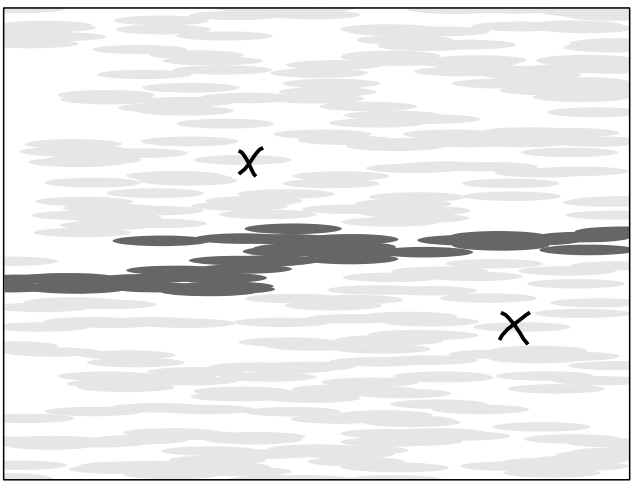

Figure 2. The result of simplified simulation for a structure induced by the impurities of an ordered phase. Grey color indicates the regions of local antiferromagnetic order, black covers the region of macroscopic order, and white corresponds to disordered regions. Two single clusters are marked by crosses.

The obtained picture of microscopic phase separation is in agreement with the results of numerical 2D Monte Carlo simulations for the ground state of spin-Peierls and Haldane systems with impurities [17]. According to this model that takes into account the interchain interaction, the antiferromagnetically correlated spin projections exist in the vicinity of spin vacancies. Away from the impurities the average values of spin projections are close to zero. Importantly, the simulation of Ref. [17] demonstrates a strong, virtually hundred percent, modulation of the order parameter. Assuming that the small order parameter in regions between the impurities will be destroyed by thermal fluctuations at finite temperatures, we conclude that the simulated structure is equivalent to that proposed based on the coexistence of two magnetic resonance signals.

3. Triangular antiferromagnets

As noted in Section 1, the antiferromagnetic exchange interaction, unlike the ferromagnetic interaction, can be frustrated as a result of the structural features of the crystal. A vivid example of this effect is antiferromagnetic structure on a plane hexagonal lattice — the so-called triangular antiferromagnets. Magnetic moments at the vertices of regular triangles cannot form an ordinary collinear structure. The minimum of the classical exchange energy is achieved if the neighboring spins are at an angle of 120° to each other. This is a doubly degenerate state. The antiferromagnetic interaction between planes in real hexagonal crystals does not violate this structure, making spins in neighboring planes align antiparallel. The static and dynamic properties of such systems depend significantly on the ratio of in-plane to interplane exchange interactions between magnetic ions, but in either case differ considerably from the properties of usual two-sublattice antiferromagnets. The largest discrepancies are for the magnetic susceptibility tensors, phase diagrams (especially ones in a magnetic field), and the number and field dependences of the magnetic resonance modes. While the study of quasi-two-dimensional systems has until recently been limited to theoretical work (see, for example, Refs [18, 19]), relatively recently the first experiments — specifically on the compound $RbFe(MoO_4)_2$ — have been made [20]. The most comprehensive review of the magnetostatic and resonant properties of this system is given in Ref. [21].

Quasi-one-dimensional triangular antiferromagnets have been studied extensively over the past two decades, both experimentally and theoretically. Such systems largely occur on crystal structures of the ABX_3-type (where A is an alkali metal, B a magnetic 3d-ion, and X a halogen) which usually belong to the space symmetry group $P6_3/mmc$ (D^4_{6h}). Magnetic ions are located on the sites of a simple hexagonal Bravais lattice, and the exchange interaction between neighbors along the six-fold axis turns out to be 10 to 100 times stronger than the interaction in the basal plane. In the ordered phase neighboring spins along the chains are antiparallel, whereas in the hexagonal planes they are at about 120° to each other. Depending on the sign of the magnetic anisotropy, the planes of the spins can lie either in the basal plane (easy-plane antiferromagnets $CsMnBr_3$, $KNiCl_3$, etc.) or in a plane containing the six-fold axis C_6 (easy-axis antiferromagnets $CsNiCl_3$, $RbNiCl_3$, $CsMnI_3$). Such systems differ widely in their magnetic properties. In this paper, the static and resonant properties of easy-axis structures are described using the example of the compound $RbNiCl_3$. From neutron-scattering experiments [22], at a temperature $T_N \simeq 11$ K this magnet acquires an ordered structure similar to a helicoidal one with wave vector $\mathbf{k} = (4\pi/3a, 0, \pi/c)$, where a and c are lattice parameters. By various estimates, the value of the intrachain exchange interaction is $J \simeq 20$ K [23], and that of the interchain interaction is $J' \simeq 2$ K [26]. The easy-axis anisotropy constant is approximately $D \simeq -0.05$ K. Because $D \ll J, J'$, the triangle exchange structure turns out to be virtually unchanged by relativistic interactions. Due to its quasi-one-dimensional nature, the magnetic structure is strongly influenced by zero-point oscillations, which reduce the average spin on the site to $1.3\mu_B$ at temperatures well below T_N.

Magnetization measurements at a temperature of 1.5 K, carried out with a standard SQUID magnetometer for two magnetic field orientations relative to the easy axis are presented in Fig. 3. Applying a magnetic field perpendicular to the C_6 axis (circles) gives rise to a virtually linear magnetization curve due to the usual canting of the antiferromagnetic sublattices towards the field. But if the field is along the easy axis (in the spin plane), then at $H = H_c \simeq 20$ kOe the curve $M(H)$ exhibits a jump due to the flop of the spin plane (spin-flop-transition). The main difference from the two-sublattice antiferromagnet is that in fields less than H_c a nonzero susceptibility due to the noncollinear structure is observed at $T \ll T_N$. The components of the susceptibility tensor are largely determined by the intrachain exchange interaction. From a simple molecular field calculation, their ratio is $\chi_\parallel = 2\chi_\perp = 1/(8J)$ (where the indices $\parallel$ and $\perp$ are introduced relative to a vector perpendicular to the spin plane). For $RbNiCl_3$ this ratio is $\chi_\parallel/\chi_\perp = 1.8$. The slightly nonlinear high-field magnetization and the different values of the $H \perp C_6$ and $H \parallel C_6$ magnetizations above the spin-flop field are due to the contribution of the zero-point oscillations [27].

The resonance spectra of various easy-axis triangular antiferromagnets have been studied in detail by many researchers [24–26, 29]. In this paper we present the results, similar to those of Ref. [26], of low-temperature spectroscopic measurements performed on a single crystal of $RbNiCl_3$ using a transmission type spectrometer in the frequency range of 30–80 GHz in magnetic field up to 40 kOe. From Fig. 4 it is

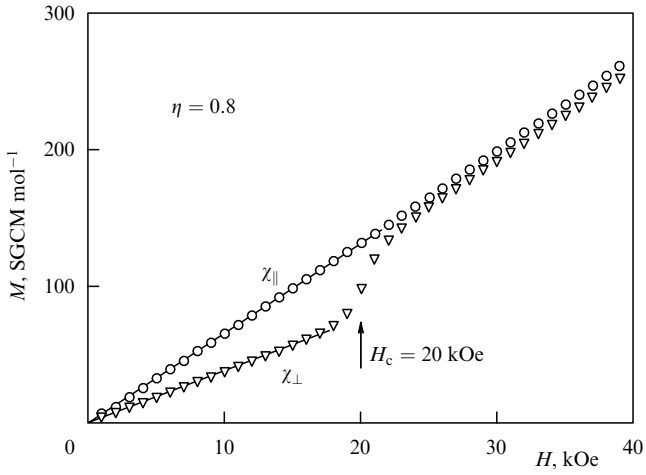

Figure 3. Field dependence of the magnetization of an $RbNiCl_3$ sample at $T = 1.5$ K. Triangles: $H \parallel C_6$, circles: $H \perp C_6$. Solid lines: linear fit for determining $\chi_\parallel$ and $\chi_\perp$. The arrow indicates the spin flop field H_c.

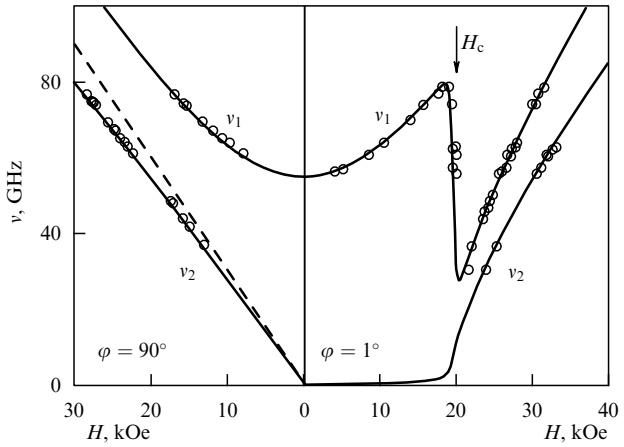

Figure 4. Frequency-field diagrams of an AFMR in $RbNiCl_3$ at $T = 1.3$ K for two magnetic field orientations relative to the C_6 axis. Solid lines are calculated from Eqn (4) with parameters $\eta = 0.8$, $H_c = 20$ kOe as determined from static measurements. The dashed line shows the paramagnetic curve $\nu = \gamma H$. The arrow indicates the value of the field of the spin-flop transition.

seen that for both major magnetic field orientations (φ is the angle between the field and the C_6 axis) the resonance spectrum consists of two branches, labeled ν_1 and ν_2, which have a complex magnetic field dependence. The gap branch ν_1 at $H \parallel C_6$ first increases, then experiences a sharp jump at $H_c = 20$ kOe, and then increases again approaching the paramagnetic dependence. The ν_2 branch remains zero up to H_c, beyond which point it increases in a similar way to ν_1. For the other orientation, both branches increase monotonically, one of them, ν_2, turning out to be close to, but clearly distinct from, the paramagnetic line $\nu = \gamma H$ (where γ is the gyromagnetic ratio).

The resonant properties of such noncollinear structures are extremely hard to analyze in terms of a microscopic spin Hamiltonian and, besides, the presence in a system of many sublattices requires numerous model restrictions to be introduced. The most adequate approach to describe the long-wave part of the resonance spectrum of such structures is to invoke the ideas of exchange symmetry [28]. The spatial spin density of a 120° magnetic structure is specified by the orthogonal unit vectors $\mathbf{l}_1, \mathbf{l}_2$ and the wave vector $\mathbf{k}$,

$$\mathbf{S} \sim \mathbf{l}_1 \cos \mathbf{kr} + \mathbf{l}_2 \sin \mathbf{kr} .$$

The long-wavelength dynamics of a magnet (neglecting its internal degrees of freedom) is specified by the motion of these vectors, and its kinetic energy in a magnetic field is determined by the quadratic form

$$E = \frac{\chi_{\alpha\beta}}{2} (\Omega + H)_\alpha (\Omega + H)_\beta ,$$

where $\chi_{\alpha\beta} = \chi_\perp \delta_{\alpha\beta} + (\chi_\parallel - \chi_\perp) n_\alpha n_\beta$ is the susceptibility tensor of the exchange structure, Ω is the angular rotation velocity in spin space, and $\mathbf{n} = [\mathbf{l}_1 \mathbf{l}_2]$ is the normal vector to the spin plane. For the interaction of the spin system with the crystal (which is weak compared to the exchange), the potential energy is represented, to a first approximation, as a quadratic form in the components $\mathbf{l}_1, \mathbf{l}_2$, which is invariant under the symmetry transformations of the exchange structure. The Lagrangian of the system is then represented in the form

$$\mathcal{L} = E - \frac{\alpha}{2} n_z^2 . \tag{3}$$

For a magnetic field at an arbitrary angle φ to the easy axis, the equilibrium orientation of the spin plane, which is specified by the angle ψ between the vector $\mathbf{n}$ and the easy axis, is determined by

$$\tan 2\psi = \frac{H^2 \sin 2\varphi}{H^2 \cos 2\varphi - H_c^2} ,$$

where $H_c^2 = \alpha/(\chi_\parallel - \chi_\perp)$ is the spin plane flop field for $\mathbf{H}$ along the easy axis ($\varphi = 0$).

Expanding the vectors $\mathbf{n}$ and $\mathbf{\Omega}$ in the Lagrangian (3) to second order in the small off-equilibrium angle θ and varying the resulting expression, we obtain a secular equation for the eigenfrequencies,

$$\begin{vmatrix} \omega^2 - \eta P & \mathrm{i}\omega(1-\eta) Z \\ -\mathrm{i}\omega(1-\eta) Z & \omega^2 - \eta Q \end{vmatrix} = 0 , \tag{4}$$

where

$$Q = \sqrt{H^4 - 2H^2 H_c^2 \cos 2\varphi + H_c^4} ,$$

$$P = \frac{1}{2}(Q - H_c^2 + H^2) ,$$

$$Z = H \cos(\psi - \varphi) , \qquad \eta = \frac{\chi_\parallel - \chi_\perp}{\chi_\perp} .$$

The first calculation of this type was performed in Ref. [25]. As seen from Eqn (4), as few as two phenomenological parameters, η and H_c, are sufficient to describe the spectrum of an AFMR, the selfconsistency of the approach being emphasized by the fact that these parameters are determined independently from magnetostatic measurements. The results of calculations from Eqn (4) with $\eta = 0.8$, $H_c = 20$ kOe, which are shown by solid lines in Fig. 4, are in excellent agreement with experiment.

Two relativistic branches of the spectrum, ν_1 and ν_2, are associated with the oscillations of the spin plane (vector $\mathbf{n}$) with respect to the crystal and the magnetic field. Clearly, a plane noncollinear structure must also have a third relativistic branch in its spectrum, one associated with the uniform rotations of spins in the plane (about the vector $\mathbf{n}$). If the anisotropic distortion of the triangular structure is small, such a degree of freedom is practically degenerate, making this branch unobservable in $RbNiCl_3$. To describe larger anisotropies, one should introduce the relativistic invariants of higher order in the components $\mathbf{l}_1, \mathbf{l}_2$, which lift the in-plane degeneracy of the spin structure. This was first done to describe the lower branch of the AFMR spectrum in the antiferromagnet $CsMnI_3$ [29] and diamagnetically diluted $RbNi_{1-x}Mg_xCl_3$ [30].

To summarize, the noncollinear magnetic ordering arising due to the weak geometric frustration of exchange interaction in hexagonal crystals has rather unusual properties. The most interesting properties manifest themselves in the long-wavelength spin dynamics, which differs from that in the collinear case in both the type of oscillations and the number of magnetic resonance modes, as well as in their evolution in an external magnetic field. Additional interest in these problems comes from the fact that these effects allow a self-

consistent description in terms of the symmetric 'hydrodynamical' approach which is free of any model restrictions [28].

4. Strongly frustrated ferromagnets

The weakly frustrated exchange interaction considered in Section 3 does not prevent the formation of the Néel state. There exist, however, crystal lattices (such as kagome, garnet, and pyrochlore) whose exchange interaction is not capable of stabilizing any ordering. Over the last decade, several such systems have been investigated [31]. In this paper we limit ourselves to considering the magnetic properties of the pyrochlore antiferromagnet $Gd_2Ti_2O_7$. The magnetic ions Gd^{3+} ($S = 7/2$, $L = 0$) in this crystal form a face-centered cubic Bravais lattice with a regular tetrahedron as a basis (the projection of the lattice on the [111] crystal plane is shown schematically in Fig. 5). The magnetic ground state of such a structure must, in the nearest-neighbor-exchange approximation, satisfy the condition that the total spin on each tetrahedron be zero — but such classical states prove to be infinite in number. The fluctuations between various states that are practically degenerate in energy lead to the consequence that the spin system remains disordered down to $T = 0$ [32, 33]. Heat capacity and magnetic susceptibility measurements [34–36] and neutron experiments [37] have recently shown that $Gd_2Ti_2O_7$ indeed remains disordered over a wide range of temperatures below the Curie–Weiss temperature $\theta_{CW} \simeq 10$ K. The transition to the ordered phase, presumably due to the dipole–dipole interaction, occurs only at a temperature $T_{N1} \approx 1$ K.

The infinite degeneracy of the ground state of a frustrated magnet is equivalent to the existence of a macroscopic number of local soft modes in its excitation spectrum, which corresponds to the rotational degrees of freedom of the spins located at the vertices of the hexagons the edges of the neighboring tetrahedra form in the kagome plane (see Fig. 5). If spins are ordered antiparallel along the perimeter of a hexagon, then in the absence of an external field their rotation through an arbitrary angle in spin space does not change the total exchange energy of the system. Such low-lying modes were observed in the quasi-elastic neutron scattering in $ZnCr_2O_4$, another Heisenberg antiferromagnet on a pyrochlore lattice [38].

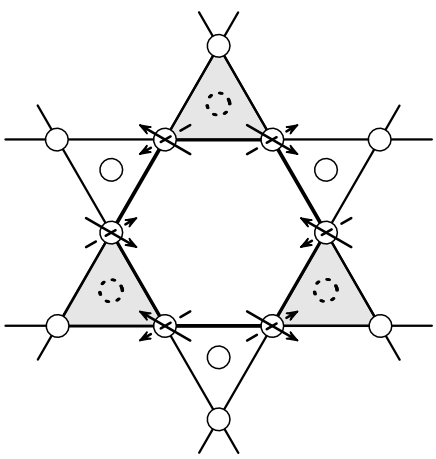

Figure 5. Schematic of the pyrochlore crystal lattice as projected onto the [111] plane. Grey and white triangles indicate, respectively, down- and up-pointing tetrahedra with magnetic ions in their vertices. The solid line traces out the hexagon formed by the faces of the neighboring tetrahedra. The arrows indicate the antiferromagnetic ordering of magnetic moments on the hexagon.

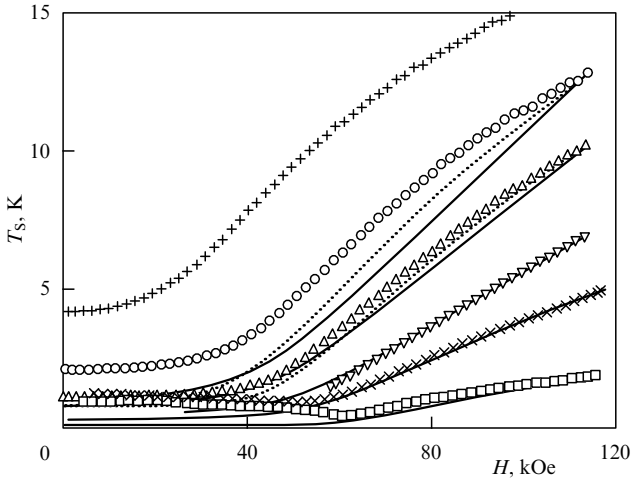

Figure 6. Dependence of the temperature of a $Gd_2Ti_2O_7$ sample on the magnetic field parallel to the [111] plane as the sample is quasi-adiabatically demagnetized from a field of 118 kOe, for various starting temperatures T_i. Solid lines: Monte Carlo simulation, dotted lines: demagnetization curves corrected for the lattice heat capacity.

Thermodynamically, the existence of soft modes manifests itself most importantly in that much of magnetic entropy shows no freeze-out down to well below θ_{CW}. The modes persist up the saturation field H_{sat} (in $Gd_2Ti_2O_7$ $H_{sat} \simeq 70$ kOe) and then acquire a Zeeman gap. The transition from the nondegenerate, fully polarized state that exists above H_{sat} to the infinitely degenerate state below H_{sat} occurs through the 'condensation' of a macroscopic number of local modes and is accompanied by a large change in entropy in the vicinity of the critical field [39]. This property suggests the existence in $Gd_2Ti_2O_7$ of the enhanced magnetocaloric effect which was recently investigated in Ref. [40]. Figure 6 presents the magnetic field dependence of the temperature of a sample of $Gd_2Ti_2O_7$ as it is quasi-adiabatically demagnetized starting from various temperatures T_i. All the $T_S(H)$ lines starting from 10 K and below exhibit a sharp temperature drop in the field range of 120–60 kOe (in contrast to the uniform $T/H =$ const cooling of an ideal paramagnet), with the maximum value of the initial-to-final temperature ratio T_i/T_f exceeding 10. This experiment clearly demonstrates the fundamental role of strong exchange frustration in the magnetic cooling of $Gd_2Ti_2O_7$. A quantitative description of the obtained data was performed by Monte Carlo simulation of a classical antiferromagnet in the nearest-neighbor approximation (for a detailed description see Ref. [39]). The exchange constant J, the only parameter needed for fitting the simulated to experimental results, can be estimated from the saturation field and the Curie–Weiss temperature, whose values for a pyrochlore magnet, in the molecular field approximation, are given by (see, for example Ref. [39])

$$g\mu_B H_{sat} = 8JS\,, \qquad k_B\theta_{CW} = 2JS(S+1)\,. \tag{5}$$

From either of Eqns (5), $J \simeq 0.3$ K. Solid lines in Fig. 6 present simulation results for this value of J which, taking into account the high-temperature corrections for the lattice heat capacity (as shown dashed) are in excellent agreement

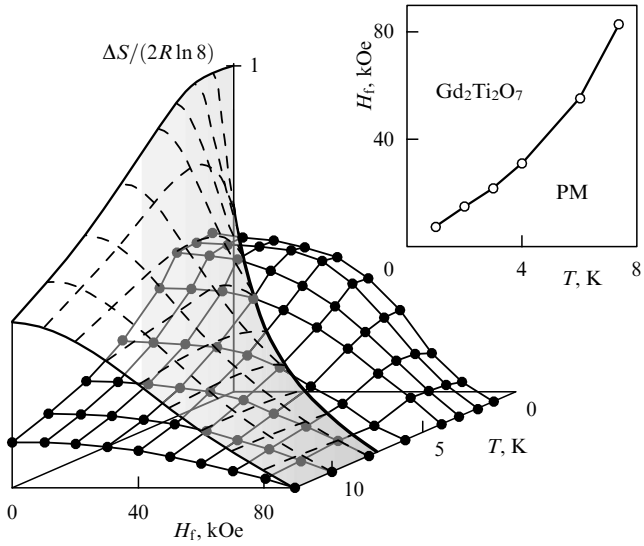

Figure 7. Entropy change in $Gd_2Ti_2O_7$ isothermally demagnetized from $H_i = 90$ kOe, as a function of the final H_f for various temperatures. Grey surface with dashed lines: similar calculations for an ideal spin-7/2 paramagnet. Inset shows the boundary in the $H_f - T$ plane between the regions of preferentially demagnetized pyrochlore and ideal paramagnet (PM).

with experiment — thus directly validating the use of the concept of soft modes in the thermodynamic description of a frustrated magnet.

In concluding this section, we can estimate the cold-productivity of the process based on the adiabatic demagnetization curves $T_S(H)$ given above and using the heat capacity data $C(T)$ for antiferromagnet $Gd_2Ti_2O_7$ obtained with the Quantum Design calorimeter in a strong magnetic field $H = 90$ kOe in the temperature range of 1.5–20 K. For an isothermally demagnetized magnet, the heat it absorbs and its change in entropy are related by the simple relation

$$\Delta Q = T\Delta S\Big|_{H_i}^{H_f}.$$

Let us consider the adiabatic demagnetization curve as it goes from the initial point (H_i, T_i) to the final point (H_f, T_f). Because the entropy remains constant along the curve, the entropy change at a constant temperature T_f and that at a fixed field H_i are related by

$$\Delta S(T_f)\Big|_{H_i}^{H_f} = \Delta S(H_i)\Big|_{T_f}^{T_i} = \int_{T_f}^{T_i} \frac{C(T)}{T}\,\mathrm{d}T. \qquad (6)$$

The values of $\Delta S|_T$ calculated from Eqn (6) for demagnetization from the field $H_i = 90$ kOe to the final value H_f at various temperatures are indicated by full circles in Fig. 7 (note that the total entropy of the system remains indefinite). There are two key points to be made here: (1) even at temperatures close to the ordering temperature $T_{N1} = 1$ K the system conserves about half of the total magnetic entropy $2R\ln 8$, and (2) the changes in entropy and heat absorption are a maximum in the strong field region above H_{sat}. This is quite different from the low-temperature behavior of a conventional paramagnet (as shown dashed on the grey surface in Fig. 7), whose entropy is released only at demagnetization down to $H_f \ll H_i$. The $H_f - T$ plot in the inset of Fig. 7 shows the boundary of the region in which the entropy of $Gd_2Ti_2O_7$ changes faster than that of an ideal paramagnet. The cold productivity ΔQ reaches a maximum of 30 J mol^{-1} near 4 K. This amount of heat corresponds to the evaporation heat of a mole of liquid ^{3}He at $T = 3$ K, thus offering the possibility, in principle, of using the pyrochlore magnet $Gd_2Ti_2O_7$ in cryogenic applications.

5. Conclusion

In conclusion, this paper discusses several types of strongly correlated, insulating spin systems with antiferromagnetic exchange interaction in which, unlike conventional magnetic crystals, low-temperature spin order occurs in an unusual way, if at all. In disordered low-temperature structures, new effects, such as magnetic order induced by nonmagnetic impurities, appear. At the critical point for the appearance of this nontrivial ordering, macroscopic phase separation is experimentally observed to occur in the magnetic states of the insulating matrix.

Antiferromagnetic exchange interaction on a hexagonal lattice, if it is geometrically frustrated, can lead to exotic noncollinear triangle magnetic structures with interesting dynamic properties; these properties have been the subject of much study, both experimentally and theoretically. A high level of frustration — such as in a pyrochlore lattice magnet — not only rules out usual ordering but also fully destroys long-range order and leads to a new collective paramagnetic state of the spin liquid type, with unique thermodynamics in a magnetic field. There are prospects for cryogenic applications of the enhanced magnetocaloric effect observed in such systems. Further study of such systems is apparently high on the agenda for the physics of magnetic phenomena.

Acknowledgements. The authors thank V N Glazkov, M E Zhitomirskiĭ, V I Marchenko, and O A Petrenko for their advice and encouragement. The provision of samples by S V Petrov, G Balakrishnan, T Masuda, and K Uchinokura is gratefully acknowledged.

References

1. Bethe H *Z. Phys.* **71** 205 (1931)
2. Haldane F D M *Phys. Rev. Lett.* **50** 1153 (1983)
3. Villain J *Z. Phys. B* **33** 31 (1979)
4. Dagotto E, Rice T M *Science* **271** 618 (1996)
5. Kageyama H et al. *Phys. Rev. Lett.* **82** 3168 (1999)
6. Garrett A W et al. *Phys. Rev. Lett.* **79** 745 (1997)
7. Hase M, Terasaki I, Uchinokura K *Phys. Rev. Lett.* **70** 3651 (1993)
8. Pytte E *Phys. Rev. B* **10** 4637 (1974)
9. Bulaevskiĭ L N *Fiz. Tverd. Tela* **11** 1132 (1969) [*Sov. Phys. Solid State* **11** 921 (1969)]
10. Fukuyama H, Tanimoto T, Saito M *J. Phys. Soc. Jpn.* **65** 1182 (1996)
11. Shender E F, Kivelson S A *Phys. Rev. Lett.* **66** 2384 (1991)
12. Regnault L P et al. *Europhys. Lett.* **32** 579 (1995)
13. Uchiyama Y et al. *Phys. Rev. Lett.* **83** 632 (1999)
14. Oosawa A, Ono T, Tanaka H *Phys. Rev. B* **66** 020405(R) (2002)
15. Glazkov V N et al. *Phys. Rev. B* **65** 144427 (2002)
16. Shante V K S, Kirkpatrick S *Adv. Phys.* **20** 325 (1971)
17. Yasuda C et al. *Phys. Rev. B* **64** 092405 (2001)
18. Chubukov A V, Golosov D I *J. Phys.: Condens. Matter* **3** 69 (1991)
19. Gekht R S, Bondarenko I N *Zh. Eksp. Teor. Fiz.* **111** 627 (1997) [*JETP* **84** 345 (1997)]
20. Inami T, Ajiro Y, Goto T *J. Phys. Soc. Jpn.* **65** 2374 (1996)
21. Svistov L E et al. *Phys. Rev. B* **67** 094434 (2003)
22. Yelon W B, Cox D E *Phys. Rev. B* **6** 204 (1972)
23. Achiwa N *J. Phys. Soc. Jpn.* **27** 561 (1969); Iio K, Hyodo H, Nagata K *J. Phys. Soc. Jpn.* **49** 1336 (1980)
24. Tanaka H et al. *J. Phys. Soc. Jpn.* **57** 1153 (1988)

25. Zaliznyak I A at al. *Pis'ma Zh. Eksp. Teor. Fiz.* **47** 172 (1988) [*JETP Lett.* **47** 211 (1988)]
26. Petrenko O A, Petrov S V, Prozorova L A *Zh. Eksp. Teor. Fiz.* **98** 727 (1990) [*Sov. Phys. JETP* **71** 406 (1990)]
27. Zaliznyak I A *Solid State Commun.* **84** 573 (1992)
28. Andreev A F, Marchenko V I *Usp. Fiz. Nauk* **130** 39 (1980) [*Sov. Phys. Usp.* **23** 21 (1980)]
29. Abarzhi S I et al. *Zh. Eksp. Teor. Fiz.* **104** 3232 (1993) [*JETP* **77** 521 (1993)]
30. Zhitomirskiĭ M E et al. *Zh. Eksp. Teor. Fiz.* **108** 343 (1995) [*JETP* **81** 185 (1995)]
31. Ramirez A P "Geometrical Frustration", in *Handbook of Magnetic Materials* Vol. 13 (Ed. K H J Buschow) (Amsterdam: Elsevier, 2001) p. 423
32. Moessner R, Chalker J T *Phys. Rev. Lett.* **80** 2929 (1998)
33. Canals B, Lacroix C *Phys. Rev. B* **61** 1149 (2000)
34. Raju N P et al. *Phys. Rev. B* **59** 14489 (1999)
35. Ramirez A P et al. *Phys. Rev. Lett.* **89** 067202 (2002)
36. Bonville P et al. *J. Phys.: Condens. Matter* **15** 7777 (2003)
37. Champion J D M et al. *Phys. Rev. B* **64** 140407(R) (2001)
38. Lee S-H et al. *Nature* **418** 856 (2002)
39. Zhitomirsky M E *Phys. Rev. B* **67** 104421 (2003)
40. Sosin S S et al. *Phys. Rev. B* **71** 094413 (2005); cond-mat/0404529